

---

# Learning Successor Features with Distributed Hebbian Temporal Memory

---

Evgenii Dzhivelikian<sup>1</sup> Petr Kuderov<sup>1,2,3</sup> Aleksandr I. Panov<sup>1,2</sup>  
<sup>1</sup>MIPT <sup>2</sup>AIRI <sup>3</sup>FRC CSC RAS  
 {dzhivelikian.ea,kuderov.pv}@phystech.edu

## Abstract

This paper presents a novel approach to address the challenge of online temporal memory learning for decision-making under uncertainty in non-stationary, partially observable environments. The proposed algorithm, Distributed Hebbian Temporal Memory (DHTM), is based on factor graph formalism and a multicomponent neuron model. DHTM aims to capture sequential data relationships and make cumulative predictions about future observations, forming Successor Features (SF). Inspired by neurophysiological models of the neocortex, the algorithm utilizes distributed representations, sparse transition matrices, and local Hebbian-like learning rules to overcome the instability and slow learning process of traditional temporal memory algorithms like RNN and HMM. Experimental results demonstrate that DHTM outperforms LSTM and a biologically inspired HMM-like algorithm, CSCG, in the case of non-stationary datasets. Our findings suggest that DHTM is a promising approach for addressing the challenges of online sequence learning and planning in dynamic environments.

## 1 Introduction

Modelling sequential data is one of the essential tasks in Artificial Intelligence as it has many applications, including decision-making and world models [1], natural language processing [2], conversational AI [3], time-series analysis [4], and video and music generation [5]. One of the classical approaches to modelling sequential data is forming a representation that stores and condenses the most relevant information about a sequence, and finding a general transformation rule of this information through the dimension of time [6–8]. We refer to the class of algorithms that use this approach as Temporal Memory (TM) algorithms, as they essentially model the cognitive ability of complex living organisms to remember the experience and make future predictions based on this memory [9–12].

This paper addresses the problem of online sequence learning for planning and decision-making under uncertainty, which can be formalized as Reinforcement Learning (RL) for a Partially Observable Markov Decision Process (POMDP) [13, 14]. Inferring the hidden state in a partially observable environment is, in effect, a sequence modelling problem as it requires processing a sequence of observations to get enough information about hidden states. One of the most efficient representations of the hidden states for discrete POMDP is the Successor Representation (SR) that disentangles hidden states and goals given by the reward function [15–17]. The Successor Features framework is an extension of the SR into continuous POMDP, which employs the same idea of value function decomposition but, instead, for features of a hidden state [18, 19]. Temporal Memory (TM) algorithms can be leveraged to make cumulative predictions about future states and their features, forming SR or SF. This work shows that the proposed algorithm, Distributed Hebbian Temporal Memory (DHTM), can effectively form SFs for navigation tasks in Gridworld and AnimalAI [20] environments.

The most prominent TM algorithms, like a Recurrent Neural Network (RNN) [21] or a Hidden Markov Model (HMM) [22], use backpropagation to capture data relationships, known for their instability due to recurrent non-linear derivatives. They also require having complete sequences of data at hand during the training. Although the gradient vanishing problem can be partially circumvented in a way, Receptance Weighted Key Value (RWKV) [23] or Linear Recurrent Unit (LRU) [24] models do, the problem of online learning, i.e., learning on non-stationary datasets, is still a viable topic. In contrast to HMM, RNN models and their descendants also lack a probabilistic theory foundation, which is beneficial for modelling sequences captured from stochastic environments [25, 26]. There is little research on TM models that can be used in fully online adaptable systems interacting with partially observable stochastic environments with access only to one sequence data point at a time, a prevalent case in Reinforcement Learning [27].

We propose a Distributed Hebbian Temporal Memory (DHTM) algorithm based on the factor graph formalism and multi-compartment neuron model. The resulting graphical structure of our model is similar to one of the Factorial-HMM [28] but with a factor graph forming online during training. An important feature of our model is that transition matrices for each factor are stored as different components (segments) of artificial neurons, which makes computations very efficient in the case of sparse transition matrices. Our TM forms sequence representations entirely online and employs only local Hebbian-like learning rules [29–31], circumventing gradient drawbacks and making the learning process much faster than gradient methods. This comes at the expense of hidden state generalization, as DHTM’s hidden state encodes each observation sequence uniquely. Different trajectories leading to the same position in partially observable Gridworld may result in different hidden states inferred by DHTM. It’s desirable if we want to store different experiences independently, like in human episodic memory [32, 33]. Moreover, we argue that generalization is unnecessary when the reward function is well-defined in observation or feature space, and it’s more efficient to use fast hash-like encodings.

The DHTM model notoriously fits Successor Features in the Reinforcement Learning setup. The proposed TM is tested as a world model [34, 35] for an RL agent architecture, navigating in a Gridworld environment and a more challenging AnimalAI testbed [36]. Our algorithm outperforms a classic LSTM and a biologically-inspired HMM-like world model CSCG [37] in online Successor Feature formation task due to a combination of fast Hebbian-like learning and sparse hidden state coding. Another advantage of our algorithm is that it allows its implementation for neuromorphic processors, using only local learning rules.

Our contribution to this work is the following:

- We propose a distributed memory model (DHTM) based on factor graph formalism and a multicompartment neural model.
- Our model stores sparse factor functions in neural segments, which significantly lessens the number of trainable parameters, and speeds up learning.
- The DHTM learns fully online, employing only local Hebbian-like rules.
- Tested as a world model for an RL agent architecture in Gridworld and AnimalAI, DHTM outperforms LSTM and CSCG in online Successor Features formation for navigation tasks.

## 2 Background

This section provides basic information about some concepts necessary to follow the paper.

### 2.1 Reinforcement Learning

This paper considers decision-making in a partially observable environment, usually formalized as a Partially Observable Decision Process [13]. A POMDP is defined as a tuple  $\mathcal{M} = (S, A, P, R, O, D, \gamma)$ , where  $S$ —state space,  $A$ —action space,  $P(s, a, s') = Pr(s' | s, a)$ —transition function,  $R(s)$ —reward function,  $O$ —observation space,  $D(a, s', o) = Pr(o | a, s')$ —sensor model and  $\gamma \in [1, 0)$ —discount factor, given a transition  $s, a \rightarrow s'$ , where  $s \in S, a \in A, o \in O$ . If  $S, A, O$  are finite,  $P, D$  can be viewed as real valued matrices, otherwise, they are conditional density functions. Here we consider deterministic rewards, which depend only on the current state, i.e.  $R(s) : S \rightarrow \mathbb{R}$ .

The task of RL is to find a policy  $\pi(a | s) : S \times A \rightarrow [0, 1]$ , which maximizes expected return  $G = \mathbb{E}[\sum_{t=0}^T \gamma^l R_t]$ , where  $T$  is an episode length. Value based methods are usually aimed to estimate Q-function given a policy  $\pi$ :  $Q^\pi(s_t, a_t) = \mathbb{E}[\sum_{l \geq t} \gamma^l R(s_{l+1}) | s_t, a_t, \pi]$ . For an optimal value function  $Q^*$ , an optimal policy can be defined as  $\pi(a | s) = \underset{a}{\operatorname{argmax}} Q^*(s, a)$ .

## 2.2 Hidden Markov Model

Partially observable Markov process can be approximated by a Hidden Markov model (HMM) with hidden state space  $H$  and observation space  $O$ .  $O$  is the same as in  $\mathcal{M}$ , but  $H$  generally is not equal  $S$ . Variables  $H_t$  represent an unobservable (hidden) approximated state of the environment which evolves over time, and observable variables  $O_t$  represent observations that depend on the same time step state  $H_t$ , and  $h_t, o_t$  are corresponding values of this random variables. For the sake of simplicity, we suppose that actions are fully observable and information about them is included into  $H_t$  variables. For the process of length  $T$  with state values  $h_{1:T} = (h_1, \dots, h_T)$  and  $o_{1:T} = (o_1, \dots, o_T)$ , the Markov property yields the following factorization of the generative model:

$$p(o_{1:T}, h_{1:T}) = p(h_1) \prod_{t=2}^T p(h_t | h_{t-1}) \prod_{t=1}^T p(o_t | h_t). \quad (1)$$

In case of discrete hidden state, a time-independent stochastic transition matrix can be learned with Baum–Welch algorithm [38], a variant of Expectation Maximization algorithm. To compute the statistics for the expectation step, it employs the forward-backward algorithm, which is a special case of sum-product algorithm [39].

## 2.3 Successor Representation

Successor Representations are such representations of hidden states from which we can linearly infer the state value given the reward function [15]. Here, we assume observation and state spaces are discrete.

$$\begin{aligned} V(h_t = i) &= \mathbb{E}[\sum_{l=0}^{\infty} \gamma^l R_{t+l+1} | h_t = i] = \\ &= \sum_{l=0}^{\infty} \gamma^l \sum_j p(h_{t+l+1} = j | h_t = i) R_j = \\ &= \sum_j \sum_{l=0}^{\infty} \gamma^l p(h_{t+l+1} = j | h_t = i) R_j = \sum_j M_{ij} R_j, \quad (2) \end{aligned}$$

where  $\gamma$  is a discount factor, vector  $\text{SR}(h = i) = \{M_{ij}\}_j$  is a Successor Representation of a state  $i$ , and  $M_{ij} = \sum_{l=0}^{\infty} \gamma^l p(h_{t+l+1} = j | h_t = i)$ .  $R_j$  is a reward for observing the state  $j$ . That is, SR can be computed by a TM that is able to predict future states. TM algorithms effectively predict observations only for a finite time horizon  $T$ . Therefore, in order to learn SR, a technique similar to TD learning in standard RL may be employed:

$$\delta_{ij} = \sum_{l=0}^T \gamma^l p(h_{t+l+1} = j | h_t = i) + \quad (3)$$

$$+ \gamma^{T+1} \sum_k M_{kj} p(h_{t+T+1} = k | h_t = i) - M_{ij},$$

$$M_{ij} \leftarrow M_{ij} + \alpha \delta_{ij}, \quad (4)$$

where  $\alpha \in (0, 1)$  is a learning rate,  $\delta_{ij}$ —TD error for SR.

In partially observable environments, however, exact state values are not known, therefore we operate with state distributions or so-called belief states [13], which are inferred from observations. In that case, state value and SR are functions of hidden state variable distribution (see details in Appendix B).

## 2.4 Sparse Distributed Representations

In our work, we design our model to operate with sparse distributed representations (SDRs) to reflect the spatiotemporal property of cortical network activity [40]. In the discrete time case, SDR is a sparse binary vector in a high-dimensional space. To encode observed dense binary patterns to SDRs, we use a biologically plausible k-WTA (k-winners take all) neural network algorithm called spatial pooler with a Hebbian-like unsupervised learning method (see details in Appendix A).

## 3 Distributed Hebbian Temporal Memory

### 3.1 Factor Graph Model

Distributed Hebbian Temporal Memory is based on the sum-product belief propagation algorithm in a factor graph (see Figure 1). Analogously to Factorial-HMM [41], we divide the hidden space  $H$  into subspaces  $H^k$ . There are four sets of random variables (RV) in the model:  $H_{t-1}^i$ —latent variables representing hidden states from the previous time step (context),  $H_t^k$ —latent variables for the current time step,  $\Phi_t^k$ —feature variables, and  $O_t^{lm}$ —observable variables. Except for  $O_t^{lm}$ , all random variables have a categorical distribution. In contrast,  $O_t^{lm}$ , are Bernoulli variables because they represent pixels from a binary input image observation. RV state values are denoted as corresponding lowercase letters:  $h_{t-1}^i, h_t^k, \varphi_t^k, o_t^{lm}$ .

Each variable  $\Phi_t^k$  is considered independent and has a separate graphical model for increased computational efficiency. However, hidden variables of the same time step are statistically interdependent in practice. We introduce their interdependence through a segment computation trick that goes beyond the standard sum-product algorithm (see Eq. 8).

The model also has three types of factors:  $M_{t-1}^i$ —messages from previous time steps,  $F_c^k$ —context factor (generalized transition matrix),  $F_e^k$ —emission factor. We assume that messages  $M_{t-1}^i$  include posterior information from the time step  $t - 1$ , therefore we don't depict observable variables for previous time steps in Figure 1.

Further, we discuss only the upper block of the graph in Figure 1, which is DHTM itself. The lower block—an encoder—is described in the Appendix A. The only requirement for the encoder is that its output should be represented as states of categorical variables (features) for the current observation.

### 3.2 Neural Implementation

The main routine of the DHTM is to estimate distributions of currently hidden state variables given by the equation 5, the computational flow of which is schematically depicted in Figure 2:

$$p(h_t^k) \propto \sum_{\Omega_k} \prod_{i \in \omega_k} M_{t-1}^i(h_{t-1}^i) F_c^k(h_t^k, \Omega_k), \quad (5)$$

where  $\Omega_k = \{h_{t-1}^i : i \in \omega_k\}$ ,  $\omega_k = i_1, \dots, i_n$ —set of previous time step RV indexes included in  $F_c^k$  factor,  $(n + 1)$ —factor size.

For computational purposes, we translate the problem to the neural network architecture with Hebbian-like learning (for biological interpretation of the model, see Appendix C). As can be seen from Figure 2, every RV can be viewed as a set of spiking neurons representing the RV's states, that is,  $p(h_t^k) = p(c_t^j = 1)$ , where  $j$ —index of a neuron corresponding to the state  $h_t^k$ . Cell activity is binary  $c_t^j \in \{0, 1\}$  (spike/no-spike), and the probability might be interpreted as a spike rate. Factors  $F_c^k$  and  $M_{t-1}^i$  can be represented as vectors, where elements are factor values for all possible combinations of RV states included in the factor. Let's denote elements of the vectors as  $f_l$  and  $m_u$  correspondingly, where  $l$  corresponds to a particular combination of  $k, h_t^k, h_{t-1}^{i_1}, \dots, h_{t-1}^{i_n}$  state values and  $u$  indexes all neurons representing states of previous time step RVs.

Drawing inspiration from biological neural networks, we group a neuron's connections into dendritic segments. A segment acts as an independent computational unit that detects a particular input pattern (a context state) defined by its own receptive field. In our model, a segment links together factor value  $f_l$ , the computational graph shown in Figure 2, and the excitation  $E_l$  induced by the segment  $l$

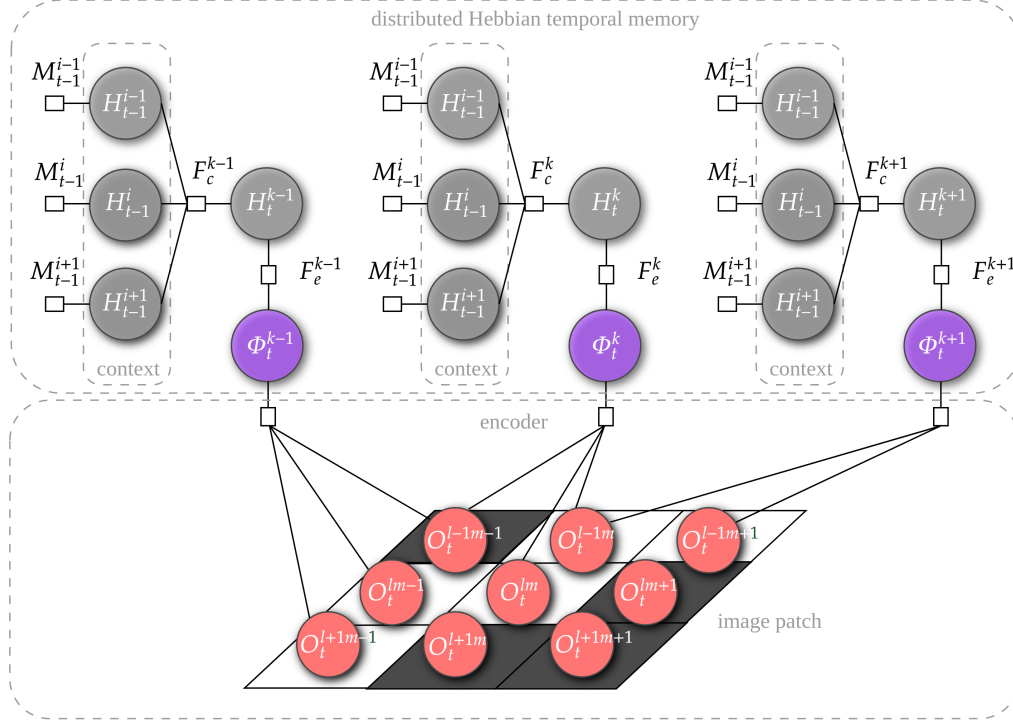


Figure 1: Partial factor graph for the DHTM. The input to the model is a sequence of binary images, each pixel is modelled as Bernoulli random variable  $O_t^{lm}$ , where  $l$  and  $m$  denote corresponding rows and cols of the image. The encoder block forms image categorical features  $\Phi_t^k$  in an unsupervised manner. Each feature  $\Phi$  has its own explaining hidden variable, which may depend on hidden variables of the other features and on itself from the previous time step.  $F_c^k$  and  $F_e^k$  are context and emission factors for the corresponding variables. Unary factors  $M_{t-1}^i$  called messages represent accumulated information about previous time steps.

to the cell it is attached to. The segment is active, i.e.,  $s_l = 1$  if all its presynaptic cells are active; otherwise,  $s_l = 0$ . Computationally, a segment transmits its factor value  $f_l$  to a cell it is attached to if the context matches the corresponding state combination.

We can now rewrite equation 5 as the following:

$$p(h_t^k) \propto \sum_{l \in \text{seg}(j)} L_l f_l^k, \quad (6)$$

where  $L_l = \prod_{u \in \text{rec}(l)} m_u$  is segment's likelihood as long as messages are normalized to probability distributions,  $\text{seg}(j)$ —indexes of segments that are attached to cell  $j$ ,  $\text{rec}(l)$ —indexes of presynaptic cells that constitute receptive field of a segment with index  $l$ .

Initially, all factor entries are zero, meaning cells have no segments. As learning proceeds, new non-zero connections grouped into segments are grown. In equation 6 we benefit from having sparse factor value vectors because its complexity depends linearly on the amount of non-zero components. And that's usually the case in our model due to one-step Monte-Carlo learning and specific form of emission factors  $F_e^k$ :

$$F_e^k(h_t^k, o_t^k) = \mathbb{I}[h_t^k \in \text{col}(\varphi_t^k)], \quad (7)$$

where  $\mathbb{I}$ —indicator function,  $\text{col}(\varphi_t^k)$  is a set of hidden states connected to the feature state  $\varphi_t^k$  that forms a column. The form of emission factor is inspired by presumably columnar structure of the neocortex and was shown to induce sparse transition matrix in HMM [37].

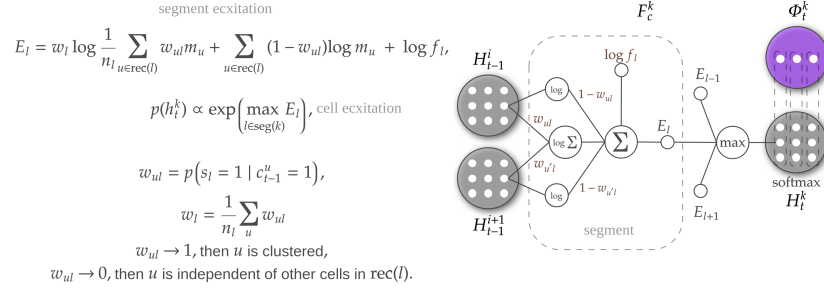


Figure 2: Neuronal implementation of the DHTM. Random variables are represented by cell clusters (white circles), where each cell corresponds to a state and its spike frequency—to the probability of the state  $p(h_t^k)$ . Cell’s dendritic segments  $\text{seg}(k)$  correspond to context factor values  $f_l$  for a particular combination of states (active presynaptic cells)  $\text{rec}(l)$ . Segments’ excitations  $E_l$  are combined to determine cell’s spike frequency  $p(h_t^k)$ . Segment’s synaptic weights reflect specificity of  $\text{rec}(l)$  combination for the segment. Emission factors  $F_e^k$  are fixed and represented by minicolumns inside a variable.

Segment likelihood  $L_l$ , resulting from the sum-product algorithm, is calculated as if presynaptic cells are independent. However, it’s not usually the case for sparse factors. To take into account, approximately, their interdependence, we substitute the following equation for segment log-likelihood:

$$\begin{aligned} \log L_l = w_l \log \frac{1}{n_l} \sum_{u \in \text{rec}(l)} w_{ul} m_u + \\ + \sum_{u \in \text{rec}(l)} (1 - w_{ul}) \log m_u, \end{aligned} \quad (8)$$

where  $w_{pl}$ —synapse efficacy or neuron specificity for segment, such that  $w_{ul} = p(s_l = 1 | c_{t-1}^u = 1)$ ,  $w_l = \frac{1}{n_l} \sum_u w_{ul}$ —average synapse efficacy for segment  $l$ , and  $n_l$ —number of cells in segment’s receptive field.

The idea that underlies the formula is to approximate between two extreme cases:

- $p(s_l = 1 | c_{t-1}^u = 1) \rightarrow 1$  for all  $u$ , which means that all cells in the receptive field are dependent and are part of one cluster, i.e., they fire together. In that case, it should be  $p(s_l) = m_u$  for any  $u$ , but we also reduce prediction variance by averaging between different  $u$ .
- $p(s_l = 1 | c_{t-1}^u = 1) \rightarrow 0$  for all  $u$  means that presynaptic cells don’t form a cluster. In that case, segment activation probability is just a product of the activation probability of each cell.

The resulting equation for belief propagation in DHTM is the following:

$$p(h_t^k) = p(c_t^j = 1) = \text{softmax} \left( \max_{j \in \text{cells}[H_t^k]} (E_j) \right), \quad (9)$$

where  $E_l = \log f_l + \log L_l$ ,  $\text{cells}[H_t^k]$ —indexes of cells that represent states for  $H_t^k$  variable. Here, we also approximate logarithmic sum with max operation inspired by the neurophysiological model of segment aggregation by cell [42].

The next step after computing  $p(h_t^k)$  distribution parameters is to incorporate information about current observations  $p(h_t^k | o_t^k) \propto p(h_t^k) \mathbb{I}[h_t^k \in \text{col}(o_t^k)]$ . After that, the learning step is performed. The step for closing the loop of our TM algorithm is to assign the posterior for the current step  $p(h_t^k | o_t^k)$  to  $M_{t-1}^i$ .

DHTM learns  $f_l$  and  $w_{ul}$  weights by Monte-Carlo Hebbian-like updates. First,  $h_{t-1}^i$  and  $h_t^k$  are sampled from their posterior distributions:  $p(h_{t-1}^i | o_{t-1}^i) \propto M_{t-1}^i$  and  $p(h_t^k | o_t^k)$  correspondingly.

---

**Algorithm 1** General agent training procedure

---

```
1: for episode=1..n do
2:   RESET_MEMORY()
3:   action ← initial_action
4:   while (not terminal) and (steps < max_steps) do
5:     obs, reward ← STEP()
6:     features ← ENCODE(PREPROCESS(obs))
7:     OBSERVE(features, action)
8:     REINFORCE(reward, features)
9:     action ← SAMPLE_ACTION()
10:    ACT(action)
11:  end while
12: end for
```

---

Then  $f_l$  is updated according to the segment's  $s_l$  and its cell's  $c_t^j$  activity so that  $f_l$  is proportional to several coincidences  $s_l = c_t^j = 1$  during the recent past, i.e., cell and its segment are active at the same time step:

$$\Delta f_l = \alpha(c_t^j - f_l)s_l, \quad (10)$$

where  $\alpha \in [0, 1)$  is segment's learning rate. That is,  $f_l$  is trained in that way that it is equal to the average cell's activation frequency, given the segment is active. It's similar to Baum-Welch's update rule [38] for the transition matrix in HMM, which, in effect, counts transitions from one state to another, but, in our case, the previous state (context) is represented by a group of RVs, not just one hidden RV.

Weights  $w_{ul}$  are also updated by the Hebbian rule to reflect the specificity of a presynaptic  $u$  for activating a segment  $l$ . That is, they are targeted to represent probability  $p(s_l = 1 \mid c_{t-1}^u = 1)$  that segment  $s_l$  is active, given cell  $u$  was active at the previous time-step. We could learn it by counting activation coincidences and mismatches. But in our algorithm it is approximated as exponential moving average of segment's  $s_l$  frequency activation, given  $c_{t-1}^u = 1$ :  $\Delta w_{ul} = \beta \cdot \mathbb{I}[c_{t-1}^u = 1] \cdot (\mathbb{I}[s_l = 1] - w_{ul})$ , where  $\beta \in [0, 1)$  — learning rate.

### 3.3 Agent Architecture

We incorporate DHTM as a part of an RL agent. We use the same agent for other memories tested as well. The agent consists of a memory model and a feature reward function. The memory model generates SF by predicting cumulative future distributions of feature variables  $\Phi^k$  according to equation 12. Here, we assume that feature representations of observations are good enough to define the reward function  $r(\varphi_t^k)$ , which is also learned during interaction with the environment and, combined with SF representations, is used to estimate the action value function. For more details on employed value function decomposition, see Appendix B.

The agent training procedure is outlined in Algorithm 1. For each episode, the memory state is reset to a fixed initial message with `RESET_MEMORY()` and `action` variable is set to a fixed initial action. An observation image returned by an environment (`obs`) is first preprocessed to get events, mimicking a simple event-based camera with a floating threshold determined from the average difference between the current and previous step image intensities. The resulting events are encoded to SDRs with a biologically inspired spatial pooling encoder described in Appendix A. In `OBSERVE()` routine, the memory learns to predict next feature states as described in Section 3. An agent learns associations to feature states and rewards in `REINFORCE()` function:

$$r_i^k \leftarrow r_i^k + \alpha \mathbb{I}[\varphi_t^k = i](R_t - r_i^k) \quad (11)$$

where  $\alpha$  is a learning rate,  $R_t$ —a reward for the current time step.

We include actions in the model by forcing some of the hidden variables  $H_t^k$  to represent actions. That is, we assume that information about action is included in the hidden state of the model. For example, if we have 4 actions, we set 4 states for one of the hidden variables and set its state from observation of the action.

In `SAMPLE_ACTION()`, for each action and current belief state, TM predicts the next belief states for which SFs of horizon  $T$  are formed using uniform strategy, i.e. setting action variable to uniform

distribution. In most experiments,  $T$  is dynamically determined from  $\Phi_{t+l}^k$  distribution. If the distribution of  $\Phi_{t+l}^k$  is close to uniform or states with high positive reward have high probability, the prediction cycle is stopped, rendering the prediction process similar to breadth-first search.

$$\begin{aligned} \text{SF}_{t+T}(\varphi^k = j \mid o_{0:t}, a_t) &= \\ &= \sum_{l=0}^T \gamma^l \sum_i p(\varphi_{t+l+1}^k = j \mid h_t^k = i) p(h_t^k = i \mid o_{0:t}, a_t) \end{aligned} \quad (12)$$

$$Q(o_{0:t}, a_t) = \sum_{jk} \text{SF}_{t+T}(\varphi^k = j \mid o_{0:t}, a_t) r_j^k, \quad (13)$$

where  $o_{0:t}$ —observation history.

## 4 Experiments

We test our model in a reinforcement learning task in Gridworld environment, where successor features are easy to interpret and the encoder block (see Sec. 3) is not required, and in a more challenging AnimalAI 3D environment. This section shows how different memory models affect SF learning and an RL agent’s adaptability. In our work, we compare the proposed DHTM model with LSTM [9] and CSCG [37]. For each setup, the results are averaged over at least five experiments with different seed values and standard deviation is shown. See Appendix D for details about baselines, their model parameters and training regimes. In Appendix E, environments and setups are more thoroughly described. The source code of experiments and algorithms’ implementations is available at <https://anonymous.4open.science/r/dhtm-D02F>.

### 4.1 Gridworld

First we test DHTM in MDP setup, that is, observation state corresponds to position in 5x5 maze. Each trial consists of two phases. In the first phase, lasting 500 episodes, there are no obstacles on the way to the terminal state that gives a reward to the agent. In the second phase, the terminal state is surrounded by a wall, so that the agent has to detour in order to get the reward, which remains in the same position. Each episode starts with the agent in the same position and ends when terminal state is entered (i.e. the reward is collected) or maximum action steps reached. Each episode, we measure the amount of action steps for agent required to reach the goal.

The results show (Fig. 3) that the agent that uses DHTM for SR formation faster converges to the optimal trajectory than CSCG. CSCG is able to converge to optimal trajectory only if the initial training dataset is gathered using random strategy after environmental changes. It requires an oracle that tells when changes occurred to gather a new training dataset. Otherwise, the agent with CSCG memory converges to suboptimal trajectories as the training batch gets very correlated trajectories following the current agent’s policy, which causes overfitting. Here, we also provide results of Q-table and SR-table agents for reference.

The second test was conducted in partially observable Gridworld in a 5x5 changing maze with a stationary terminal state as before. However, now all the agent can see is the colour of the cell in which it is located. The agent is also able to see the colour of an obstacle it encounters, receiving additional punishment.

As can be seen from Figure 4, in contrast to DHTM, CSCG and LSTM are not able to converge after reward is blocked at the 300th episode. Even with an oracle signalling about changes in the environment, which enables to gather new fully random trajectories, neither CSCG nor LSTM are able to relearn maze’s structure in online case scenario. It can be seen, however, that DHTM converges to a suboptimal trajectory of length 13 on average vs 9 steps for optimal trajectory, after reward is blocked. This may be the result of inferior generalisation properties of DHTM, which we discuss in Section 5.

In these experiments, we aimed to show that in cases of quite limited and non-stationary trajectory buffer size, an RL agent armed with DHTM memory is more adaptive than those using LSTM and



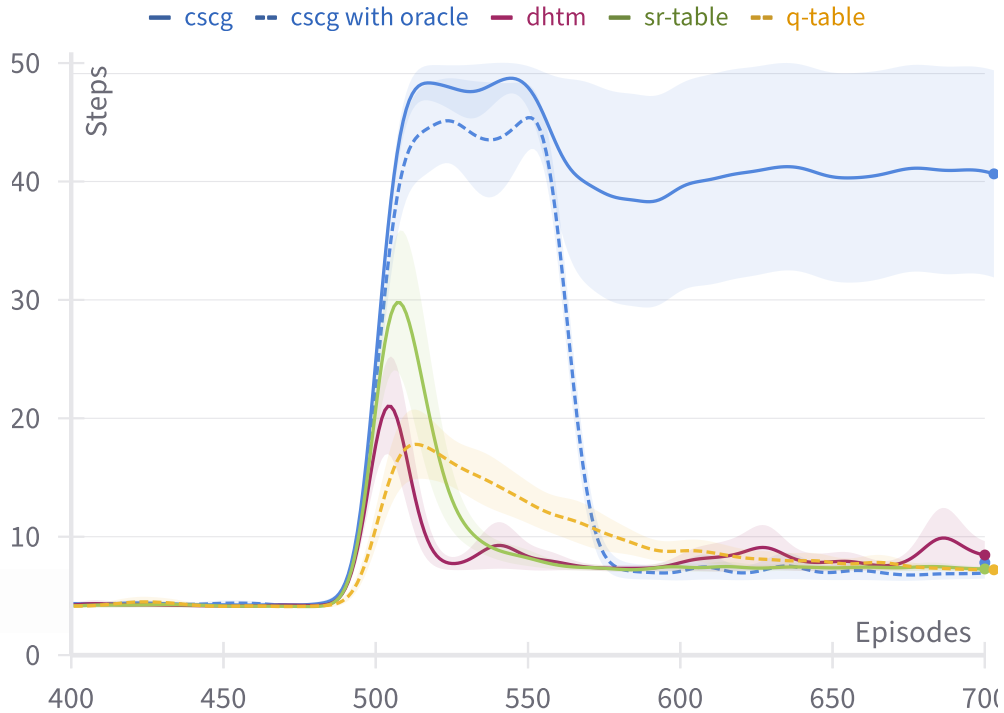


Figure 3: Amount of steps required for the agent to reach the goal in fully observable 5x5 Gridworld using different types of memory: DHTM and CSCG. CSCG is trained in two modes. The first mode is with oracle, which tells the agent to gather some trajectories using uniform policy after environment changes. The second mode is without oracle, so the agent continues using its current strategy to gather new trajectories. At the 500th episode, the terminal state is blocked by a wall, so the agent needs to find a new way to the goal. There are also plots of learning curves for Q-table and SR-table agents for reference.

CSCG. However, we do not claim that it is impossible, in principle, to train LSTM and CSCG in such a setup. We only show that DHTM notoriously fits this kind of task without numerous workarounds that would be required by those classical methods.

## 4.2 AnimalAI

AnimalAI is a 3D environment that is able to give an agent rich visual input in the form of RGB images. The objective of the experiment described here is to give a hint that DHTM is also able to deal with complex visual input due to its encoder block described in Appendix A.

The agent’s task is to reach a ball, which is food, that is located in the same room, which is 10 by 10 meters. Start agent and food positions are the same between episodes. All the agent needs to do is find the shortest path to the goal, as in the Gridworld experiments. In each episode, we measure the number of actions (steps) the agent takes to reach the goal.

The results are shown in Figure 5. We can see that after 150 episodes with the maximum number of steps set to 40, the agent stably reaches the goal. Although slight instability persists, the agent’s path is near optimal.

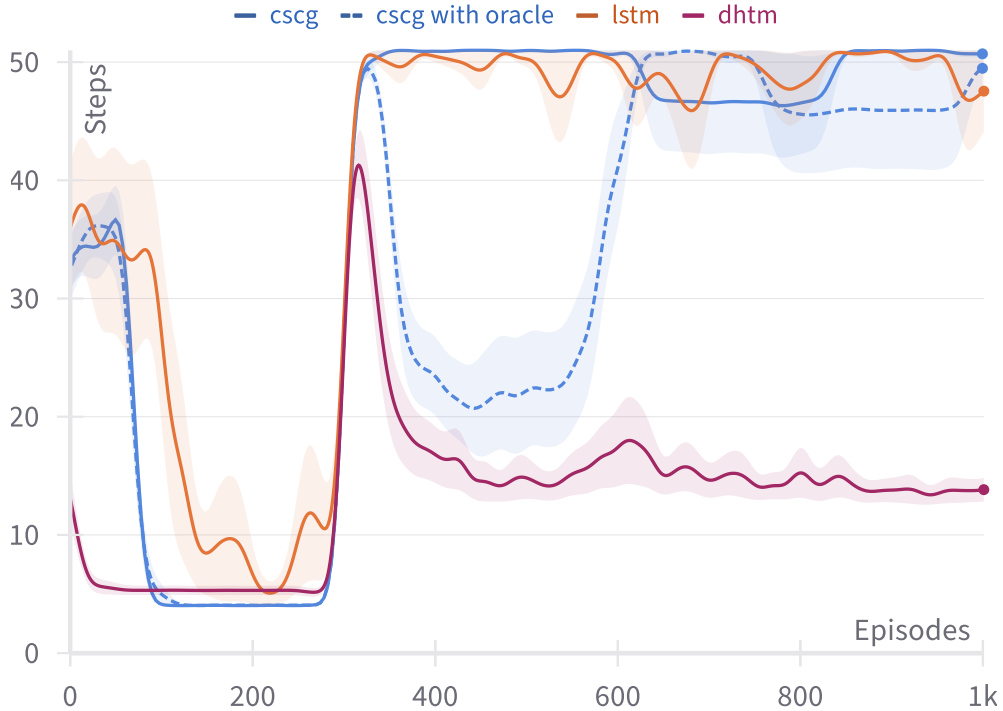


Figure 4: Learning curves measured in action steps until the goal for the agent using different memory types for SF formation in partially observable 5x5 Gridworld environment. In the 300th episode, the goal is blocked by a wall, so the agent needs to find a new optimal trajectory. CSCG is trained in two modes. The first mode is with an oracle, which tells the agent to gather some trajectories using uniform policy after the environment changes. The second mode is without an oracle, so the agent continues using its current strategy to gather new trajectories.

We weren't able to train CSCG and LSTM with the same encoder block as we used for DHTM, even after increasing their trajectory buffer sizes. We think that the problem might be because of the non-stationarity of the encoder's output, which adapts continuously.

## 5 Conclusion

This paper introduces a novel probabilistic Factorial-HMM-like algorithm, DHTM, for learning an observation sequence model in non-stationary environments that uses local Hebbian-like learning rules. DHTM is scalable to multiple feature variables by employing sparse distributed representations and sparse factor function implementation using segments, which inspire biologically plausible multicomponent neural models. In contrast to methods that use Monte-Carlo trajectory sampling for future state probability estimation, our method can perform belief propagation, so each prediction step adds a constant amount of computation, allowing a long planning horizon.

Experiments show that our memory model can quickly learn and unlearn observation sequences and transition dynamics, even in changing environments. In that case, methods that rely on backpropagation, like LSTM and CSCG, are difficult to train and require rigorous trajectory buffer management, a common problem in RL tasks.

One of the main limitations of the DHTM is that its temporal context is completely random, as it is formed on the fly using only the local information available. As a result, the mechanism of

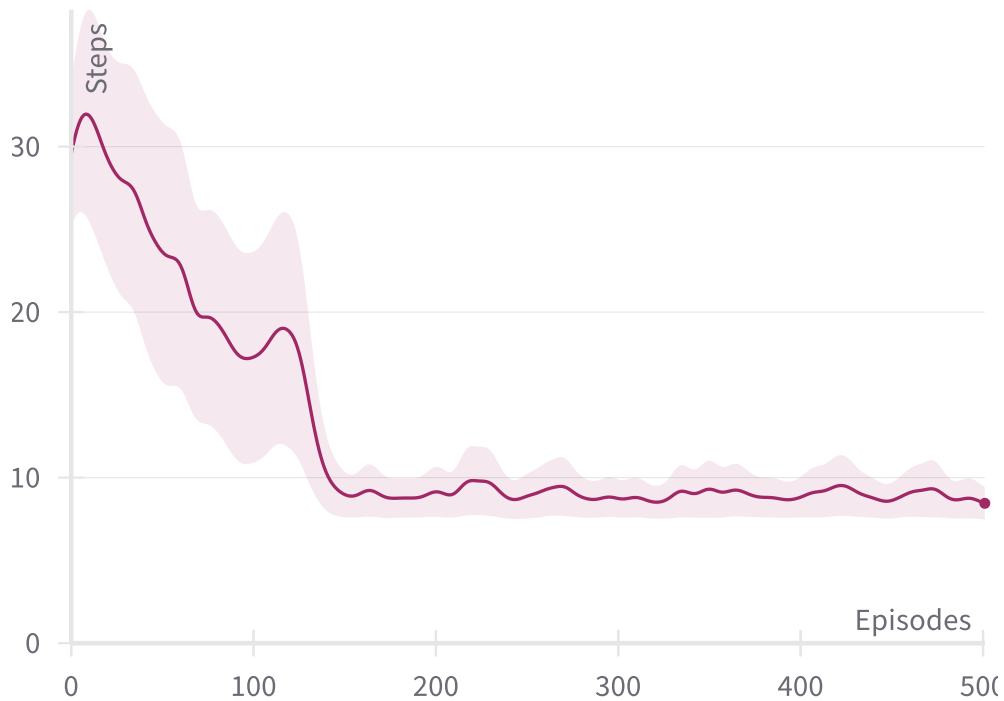


Figure 5: Amount of action steps the agent uses to reach the goal in a 10x10-meter room in AnimalAI environment using DHTM memory for SF formation. The agent and the goal have the same initial positions throughout the episodes. Each timestep, the agent gets an image of a first-person view of the environment and produces one of three actions: turn left, turn right, or go forward.

context formation allows only limited generalizations between different trajectories. However, this is what makes fast learning possible. Combining this fast learning with more slow learning that allows generalizations is a promising direction. Forming Successor Features combined with a two-level hierarchy of DHTM layers may provide the next step to a more generalized sequence model. The first (fast) DHTM layer may be used to form Successor Features both for planning and as current state representation, which is then observed by the second (slow) DHTM layer. We hypothesize that because SFs should provide a better generalization than the raw features, the second layer should be able to form a more versatile model of the environment.

## 6 Impact Statements

This paper presents research that aims to advance the field of machine learning. There are numerous potential societal consequences of our work, none of which we believe require special emphasis here.

## References

- [1] Thomas M Moerland, Joost Broekens, Aske Plaat, Catholijn M Jonker, et al. Model-based reinforcement learning: A survey. *Foundations and Trends® in Machine Learning*, 16(1):1–118, 2023.
- [2] Bonan Min, Hayley Ross, Elior Sulem, Amir Pouran Ben Veyseh, Thien Huu Nguyen, Oscar Sainz, Eneko Agirre, Ilana Heintz, and Dan Roth. Recent advances in natural language

- processing via large pre-trained language models: A survey. *ACM Computing Surveys*, 2021.
- [3] Yogesh K Dwivedi, Nir Kshetri, Laurie Hughes, Emma Louise Slade, Anand Jeyaraj, Arpan Kumar Kar, Abdullah M Baabdullah, Alex Koochang, Vishnupriya Raghavan, Manju Ahuja, et al. “so what if chatgpt wrote it?” multidisciplinary perspectives on opportunities, challenges and implications of generative conversational ai for research, practice and policy. *International Journal of Information Management*, 71:102642, 2023.
  - [4] Gökcen Eraslan, Žiga Avsec, Julien Gagneur, and Fabian J Theis. Deep learning: new computational modelling techniques for genomics. *Nature Reviews Genetics*, 20(7):389–403, 2019.
  - [5] Shulei Ji, Jing Luo, and Xinyu Yang. A comprehensive survey on deep music generation: Multi-level representations, algorithms, evaluations, and future directions. *arXiv preprint arXiv:2011.06801*, 2020.
  - [6] Zachary C Lipton, John Berkowitz, and Charles Elkan. A critical review of recurrent neural networks for sequence learning. *arXiv preprint arXiv:1506.00019*, 2015.
  - [7] GM Harshvardhan, Mahendra Kumar Gourisaria, Manjusha Pandey, and Siddharth Swarup Rautaray. A comprehensive survey and analysis of generative models in machine learning. *Computer Science Review*, 38:100285, 2020.
  - [8] Christoph Mathys, Jean Daunizeau, Karl J Friston, and Klaas E Stephan. A bayesian foundation for individual learning under uncertainty. *Frontiers in human neuroscience*, 5:39, 2011.
  - [9] Sepp Hochreiter and Jürgen Schmidhuber. Long short-term memory. *Neural computation*, 9: 1735–80, 12 1997. doi: 10.1162/neco.1997.9.8.1735.
  - [10] Karl Friston, Thomas FitzGerald, Francesco Rigoli, Philipp Schwartenbeck, Giovanni Pezzulo, et al. Active inference and learning. *Neuroscience & Biobehavioral Reviews*, 68:862–879, 2016.
  - [11] Karl J Friston, Richard Rosch, Thomas Parr, Cathy Price, and Howard Bowman. Deep temporal models and active inference. *Neuroscience & Biobehavioral Reviews*, 90:486–501, 2018.
  - [12] Thomas Parr and Karl J Friston. Working memory, attention, and salience in active inference. *Scientific reports*, 7(1):14678, 2017.
  - [13] Pascal Poupart. *Exploiting structure to efficiently solve large scale partially observable Markov decision processes*. Citeseer, 2005.
  - [14] Gautam Singh, Skand Peri, Junghyun Kim, Hyunseok Kim, and Sungjin Ahn. Structured world belief for reinforcement learning in pomdp. In Marina Meila and Tong Zhang, editors, *Proceedings of the 38th International Conference on Machine Learning*, volume 139 of *Proceedings of Machine Learning Research*, pages 9744–9755. PMLR, 18–24 Jul 2021. URL <https://proceedings.mlr.press/v139/singh21a.html>.
  - [15] Peter Dayan. Improving generalization for temporal difference learning: The successor representation. *Neural computation*, 5(4):613–624, 1993.
  - [16] Samuel J. Gershman. The Successor Representation: Its Computational Logic and Neural Substrates. *The Journal of Neuroscience*, 38(33):7193, August 2018. doi: 10.1523/JNEUROSCI.0151-18.2018. URL <http://www.jneurosci.org/content/38/33/7193.abstract>.
  - [17] Beren Millidge and Christopher L. Buckley. Successor Representation Active Inference, July 2022. URL <http://arxiv.org/abs/2207.09897>. arXiv:2207.09897 [cs].
  - [18] André Barreto, Will Dabney, Rémi Munos, Jonathan J Hunt, Tom Schaul, Hado P van Hasselt, and David Silver. Successor features for transfer in reinforcement learning. *Advances in neural information processing systems*, 30, 2017.
  - [19] Ahmed Touati, Jérémy Rapin, and Yann Ollivier. Does Zero-Shot Reinforcement Learning Exist? September 2022. URL [https://openreview.net/forum?id=MYEap\\_OcQI](https://openreview.net/forum?id=MYEap_OcQI).

- [20] Zafeirios Fountas, Noor Sajid, Pedro Mediano, and Karl Friston. Deep active inference agents using monte-carlo methods. In *Advances in Neural Information Processing Systems*, volume 33, page 11662–11675. Curran Associates, Inc., 2020.
- [21] Mikael Boden. A guide to recurrent neural networks and backpropagation. *the Dallas project*, 2(2):1–10, 2002.
- [22] Sean R. Eddy. What is a hidden markov model? *Nature Biotechnology*, 22(10):1315–1316, Oct 2004. ISSN 1546-1696. doi: 10.1038/nbt1004-1315. URL <https://doi.org/10.1038/nbt1004-1315>.
- [23] Bo Peng, Eric Alcaide, Quentin Anthony, Alon Albalak, Samuel Arcadinho, Huanqi Cao, Xin Cheng, Michael Chung, Matteo Grella, Kranthi Kiran GV, et al. Rwkv: Reinventing rnns for the transformer era. *arXiv preprint arXiv:2305.13048*, 2023.
- [24] Antonio Orvieto, Samuel L Smith, Albert Gu, Anushan Fernando, Caglar Gulcehre, Razvan Pascanu, and Soham De. Resurrecting recurrent neural networks for long sequences. *arXiv preprint arXiv:2303.06349*, 2023.
- [25] Achille Salauin, Yohan Petetin, and François Desbouvries. Comparing the modeling powers of rnn and hmm. In *2019 18th IEEE International Conference on Machine Learning and Applications (ICMLA)*, pages 1496–1499. IEEE, 2019.
- [26] Jingyu Zhao, Feiqing Huang, Jia Lv, Yanjie Duan, Zhen Qin, Guodong Li, and Guangjian Tian. Do rnn and lstm have long memory? In *International Conference on Machine Learning*, pages 11365–11375. PMLR, 2020.
- [27] Mehdi Jafarnia Jahromi, Rahul Jain, and Ashutosh Nayyar. Online learning for unknown partially observable mdps. In *International Conference on Artificial Intelligence and Statistics*, pages 1712–1732. PMLR, 2022.
- [28] Zoubin Ghahramani and Michael Jordan. Factorial hidden markov models. *Advances in neural information processing systems*, 8, 1995.
- [29] Donald Olding Hebb. *The organization of behavior: A neuropsychological theory*. Psychology press, 2005.
- [30] Patricia Smith Churchland and Terrence Joseph Sejnowski. *The computational brain*. MIT press, 1992.
- [31] Timothy P. Lillicrap, Adam Santoro, Luke Marris, Colin J. Akerman, and Geoffrey Hinton. Backpropagation and the brain. *Nature Reviews Neuroscience*, 21(6):335–346, Jun 2020. ISSN 1471-003X, 1471-0048. doi: 10.1038/s41583-020-0277-3.
- [32] Xiaohan Zhang, Lu Liu, Guodong Long, Jing Jiang, and Shenquan Liu. Episodic memory governs choices: An rnn-based reinforcement learning model for decision-making task. *Neural Networks*, 134:1–10, 2021. ISSN 0893-6080. doi: <https://doi.org/10.1016/j.neunet.2020.11.003>. URL <https://www.sciencedirect.com/science/article/pii/S0893608020303889>.
- [33] Armin W. Schulz and Sarah Robins. Episodic memory, simulated future planning, and their evolution. *Review of Philosophy and Psychology*, 14(3):811–832, Sep 2023. ISSN 1878-5166. doi: 10.1007/s13164-021-00601-1. URL <https://doi.org/10.1007/s13164-021-00601-1>.
- [34] David Ha and Jürgen Schmidhuber. World models. *arXiv preprint arXiv:1803.10122*, 2018.
- [35] Danijar Hafner, Jurgis Pasukonis, Jimmy Ba, and Timothy Lillicrap. Mastering diverse domains through world models. *arXiv preprint arXiv:2301.04104*, 2023.
- [36] Matthew Crosby, Benjamin Beyret, Murray Shanahan, José Hernández-Orallo, Lucy Cheke, and Marta Halina. The animal-ai testbed and competition. In Hugo Jair Escalante and Raia Hadsell, editors, *Proceedings of the NeurIPS 2019 Competition and Demonstration Track*, volume 123 of *Proceedings of Machine Learning Research*, pages 164–176. PMLR, 08–14 Dec 2020.

- [37] Dileep George, Rajeev V. Rikhye, Nishad Gothoskar, J. Swaroop Guntupalli, Antoine Dedieu, and Miguel Lázaro-Gredilla. Clone-structured graph representations enable flexible learning and vicarious evaluation of cognitive maps. *Nature Communications*, 12(11):2392, Apr 2021. ISSN 2041-1723. doi: 10.1038/s41467-021-22559-5.
- [38] Leonard E Baum, Ted Petrie, George Soules, and Norman Weiss. A maximization technique occurring in the statistical analysis of probabilistic functions of markov chains. *The annals of mathematical statistics*, 41(1):164–171, 1970.
- [39] F.R. Kschischang, B.J. Frey, and H.-A. Loeliger. Factor graphs and the sum-product algorithm. *IEEE Transactions on Information Theory*, 47(2):498–519, 2001. doi: 10.1109/18.910572.
- [40] Rodrigo Perin, Thomas K Berger, and Henry Markram. A synaptic organizing principle for cortical neuronal groups. *Proceedings of the National Academy of Sciences*, 108(13):5419–5424, 2011.
- [41] Z. Ghahramani and M.I. Jordan. Factorial Hidden Markov Models. *Machine Learning*, 29(2-3): 245–273, 1997. ISSN 0885-6125. doi: 10.1023/a:1007425814087.
- [42] Greg J. Stuart and Nelson Spruston. Dendritic integration: 60 years of progress. *Nature Neuroscience*, 18(12):1713–1721, Dec 2015. ISSN 1546-1726. doi: 10.1038/nn.4157. URL <https://doi.org/10.1038/nn.4157>.
- [43] Yuwei Cui, Subutai Ahmad, and Jeff Hawkins. The htm spatial pooler—a neocortical algorithm for online sparse distributed coding. *Frontiers in Computational Neuroscience*, 11:111, 2017. ISSN 1662-5188. doi: 10.3389/fncom.2017.00111. URL <https://www.frontiersin.org/article/10.3389/fncom.2017.00111>.
- [44] James Mnatzaganian, Ernest Fokoué, and Dhireesha Kudithipudi. A mathematical formalization of hierarchical temporal memory’s spatial pooler. *Frontiers in Robotics and AI*, 3, 2017. ISSN 2296-9144. URL <https://www.frontiersin.org/articles/10.3389/frobt.2016.00081>.
- [45] Petr Kuderov, Evgenii Dzhivelikian, and Aleksandr I Panov. Stabilize sequential data representation via attraction module. In *International Conference on Brain Informatics*, pages 83–95. Springer, 2023.
- [46] Matthias Oster, Rodney Douglas, and Shih-Chii Liu. Computation with spikes in a winner-take-all network. *Neural Computation*, 21(9):2437–2465, 09 2009. doi: 10.1162/neco.2009.07-08-829.
- [47] Damir Dobric, Andreas Pech, Bogdan Ghita, and Thomas Wennekers. On the importance of the newborn stage when learning patterns with the spatial pooler. *SN Computer Science*, 3(2):179, 2022.
- [48] Jochen F. Staiger and Carl C. H. Petersen. Neuronal circuits in barrel cortex for whisker sensory perception. *Physiological Reviews*, 101(1):353–415, 2021. doi: 10.1152/physrev.00019.2019. URL <https://doi.org/10.1152/physrev.00019.2019>. PMID: 32816652.
- [49] V. Mountcastle. The columnar organization of the neocortex. *Brain*, 120(4):701–722, April 1997. ISSN 14602156. doi: 10.1093/brain/120.4.701. URL <https://academic.oup.com/brain/article-lookup/doi/10.1093/brain/120.4.701>.
- [50] Adam Paszke, Sam Gross, Francisco Massa, Adam Lerer, James Bradbury, Gregory Chanan, Trevor Killeen, Zeming Lin, Natalia Gimelshein, Luca Antiga, Alban Desmaison, Andreas Kopf, Edward Yang, Zachary DeVito, Martin Raison, Alykhan Tejani, Sasank Chilamkurthy, Benoit Steiner, Lu Fang, Junjie Bai, and Soumith Chintala. Pytorch: An imperative style, high-performance deep learning library. In *Advances in Neural Information Processing Systems* 32, pages 8024–8035. Curran Associates, Inc., 2019.
- [51] Antoine Dedieu, Nishad Gothoskar, Scott Swingle, Wolfgang Lehrach, Miguel Lázaro-Gredilla, and Dileep George. Learning higher-order sequential structure with cloned hmms. (arXiv:1905.00507), May 2019. URL <http://arxiv.org/abs/1905.00507>. arXiv:1905.00507 [cs, stat].

## A Encoding and Decoding Observations

Because our model is designed to work with sparse distributed representations and the testing environments do not provide observations as SDRs by default, an encoding procedure is required. For this task, we use a modified version of the Spatial Pooler (SP) [43, 44], a distributed noise-tolerant online clustering neural network algorithm that converts input binary patterns into SDRs with fixed sparsity while retaining pairwise similarity [45]. The SP algorithm learns a spatial specialization of neurons’ receptive fields using the local Hebbian rule and  $k$ -WTA ( $k$  winners take all) inhibition [46]. Here we outline the main differences from the “vanilla” version of the SP algorithm described in Cui et al. [43].

During an agent’s decision-making process pipeline, the SP encoder accepts a current observation  $o$  and transforms it to a latent state SDR  $z$ . Observation  $o$  should be an array of binary states. To transform an RGB image into a binary array, we perform the following processing steps, simulating a simple event-based camera:

1. Transform image to greyscale.
2. Calculate difference between current and previous greyscale image  $d$ .
3. Determine average difference over the entire image  $\tau = \text{mean}(d)$ .
4. For pixels that have  $d$  above  $\tau$  set 1, for others set 0.

In terms of processing, our SP encoder functions as a standard artificial neural network with a  $k$ -WTA binary activation function.:

$$\text{overlaps}_i = \beta_i W_i o \tag{14}$$

$$z_i = \mathbb{I}[i \in \text{kWTA}(\text{overlaps})], \tag{15}$$

where  $o$ —a binary observation vector,  $W_i$ —a row-vector representing  $i$ -th neuron’s connection weights (where non-existing connections have zero weights),  $\text{overlaps}_i$ —a value representing the strength of the input pattern recognition with the neuron  $i$ <sup>1</sup>,  $\beta_i$ —an  $i$ -th neuron boosting value,  $z_i$ —an  $i$ -th bit of an output SDR,  $\mathbb{I}[\dots]$ —an indicator function, kWTA—a  $k$ -winners-take-all activation function returning  $k$  indices of the neurons with the highest overlap.

One difference between the “vanilla” SP algorithm and ours is that we do not distinguish between potential and active neural connections. Because all [existing] connections are active, they all participate in calculating overlaps. In the overlaps calculation, non-binary, that is, real-valued weights are used, similar to artificial neural networks, as shown in equation 14. Furthermore, each neuron has a fixed capacity to produce neurotransmitters, which it distributes between its synaptic connections. This means that we keep all neuron weights normalized and summed to one. While it achieves the same Hebbian learning with homeostatic plasticity as the original SP, the exact formula is slightly different:

$$\begin{aligned} \tilde{W}_i &= W_i + \alpha z_i \frac{\text{RF}_i \odot o}{\sum_j \text{RF}_j \odot o} \\ W_i &\leftarrow \frac{\tilde{W}_i}{\sum_j \tilde{W}_j}, \end{aligned} \tag{16}$$

where  $\tilde{W}_i$ —a row of new  $i$ -th neuron weights before normalization,  $\alpha$ —learning rate,  $z_i$ —a binary value representing the current activity state of the  $i$ -th neuron,  $\text{RF}_i$ —an  $i$ -th row of the binary connectivity matrix representing an  $i$ -th neuron receptive field,  $\odot$ —elementwise product,  $o$ —a binary observation vector.

The original SP algorithm has several drawbacks, including encoding instability caused by an innate homeostatic plasticity mechanism known as boosting, which helps neurons specialize and increases overall adaptability but makes memorization tasks more difficult, and slow processing on large inputs

<sup>1</sup>While the name “overlap” does not exactly reflect its meaning in our SP modification, because it is not a binary overlap between a receptive field and an input pattern, we kept it on purpose to refer to the similar term commonly used for the original SP.

such as images, where an encoding overhead becomes noticeable when compared to overall model timings around 1k input size.

The introduction of the newborn stage, which follows the ideas proposed in Dobric et al. [47], solves an encoding instability problem. The newborn stage of a spatial pooler occurs during the early stages of its learning process, when its neurons are expected to specialize. The boosting, which is intended to aid in the specialization process, is activated only during the newborn stage and its scale gradually decreases from the configured value to zero. Boosting remains turned off during an encoder’s “adulthood”, reducing the possibility of spontaneous re-specialization.

To reduce processing overhead, we use a much more sparsified connection matrix than in the original SP version. We randomly initialize connections with 40-60% sparsity, which is typical for the “vanilla” SP. Then, during the newborn stage, we gradually prune the vast majority of the weakest connections, resulting in neurons that are highly specialized due to their small receptive fields. We typically configure the final receptive field size in relation to the average input pattern size (usually 25-200% of it, resulting in 0.1-10% connections sparsity). For example, if binary input patterns have on average 100 active bits out of 1000, we can set the target size of receptive fields to 25, which is 25% of the active input size and corresponds to 2.5% connection matrix sparsity. As a result, the spatial pooler’s instability (and thus adaptiveness!) becomes even more limited in the adult stage.

Because of its soft discretization (from the distributed representation) and clusterization properties, we expect SP to assist the model with input sequence memorization and an environment transition dynamics generalization tasks in addition to the encoding itself. However, because the SP encoder learns online, particularly during the newborn stage, its output representation can be highly unstable during the early stages, potentially resulting in a performance drop.

To visualize and debug an encoded observation, we also learn a decoder, which is a linear neural layer learned locally with gradient descend on the MSE error between the predicted reconstruction and the actual observation.

## B Value Function Decomposition

In our agent model, we approximate the reward function  $R(s)$  as a sum:  $R_t = \frac{1}{n} \sum_{k=1}^n r(\varphi_t^k) \varphi_t^k$ , where  $r(\varphi_t^k)$  is a reward associated with state  $\varphi_t^k$ ,  $n$ —number of feature variables. Then, similarly to the Successor Representation idea (see Section 2.3), the value function can be represented as:

$$\begin{aligned}
 V(h_t) &= \mathbb{E}[\sum_{l=0}^{\infty} \gamma^l R_{t+l+1} | h_t] = \sum_{l=0}^{\infty} \gamma^l \mathbb{E}[\frac{1}{n} \sum_{k=1}^n r(\varphi_{t+l+1}^k) | h_t] \\
 &= \frac{1}{n} \sum_{k=1}^n \sum_j \sum_{l=0}^{\infty} \gamma^l p(\varphi_{t+l+1}^k = j | h_t^k) r_j^k \\
 &= \frac{1}{n} \sum_{k=1}^n \sum_j M_j^k(h_t^k) r_j^k, \tag{17}
 \end{aligned}$$

where  $M_j^k(h_t^k) = \sum_{l=0}^{\infty} \gamma^l p(\varphi_{t+l+1}^k = j | h_t^k)$ ,  $h_t = (h_t^1, \dots, h_t^n)$ —hidden state vector of variables  $\{H_t^k\}_k$ .

## C Biological Interpretation

Neural implementation of the DHTM is inspired by neocortical neural networks (see Fig. 6). Hidden variables  $H^k$  may be considered as populations of excitatory pyramidal neurons in cortical layer L2/3 of somatosensory areas, with lateral inhibition modelled as softmax function. Staiger and Petersen [48] showed that neurons in this layer are responsible for temporal context formation.

The neuronal activity at timestep  $t$  can be thought to carry messages  $M_{t-1}^k$ . Messages are propagated through synapses of dendritic segments, which correspond to factors  $F_c^k$ . Dendritic segments of biological neurons are known to be coincidence detectors of its synaptic input [42]. We use the notion



of dendritic segment to sparsely represent context factors  $F_c^k$ , as each factor value corresponds to a particular combination of states (or active cells).

Feature variables  $\Phi_t^k$  may be considered to represent cells of a granular layer (L4), as they are known to be the main hub for sensory excitation for L2/3. L2/3 cells that have common sensory input from the layer L4 are modelled as columns for particular feature states  $\text{col}(\varphi_t^k)$  [49].

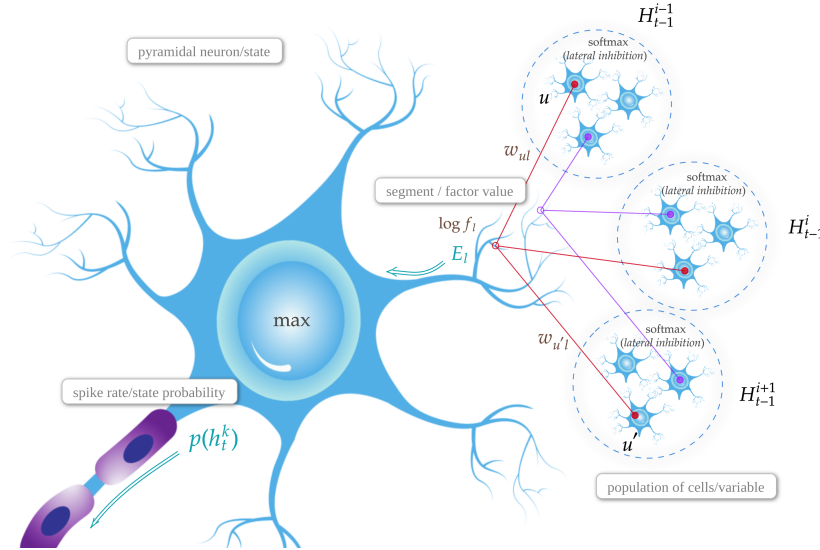


Figure 6: Biological view of the neural implementation of the DHTM. Variables  $H_{t-1}^i$  correspond to populations of neurons that have common sensory input and lateral inhibitory competition. Dendritic segments correspond to factor values  $f_i$ . spike frequency of a neuron reflects state probability  $p(h_t^k)$  of a variable.

## D Implementation details

As mentioned in Section 3.3, we incorporate DHTM as a part of an RL agent, which has a memory model and a feature reward function. All tested memory models share the same pipeline—they learn sequences of encoded binary observations (i.e. SDRs that we get from Spatial Pooler encoder described in Appendix A) concatenated with one-hot encoded actions.

### D.1 LSTM

LSTM baseline was implemented with a single LSTMCell from PyTorch library [50]. It is supported by an additional symexp-layer to encode input before passing it to the LSTM cell and a symexp-layer to decode the LSTM cell's output from the LSTM's hidden state back to the input representation, where symexp activation function,  $\text{symexp}(x) = \text{sign}(x)e^{|x|-1}$ , is a reverse of symlog function:  $\text{symlog} = \text{sign}(x) \log(|x| + 1)$ .

For the Gridworld task, LSTM with a hidden state size of 100 is trained on a buffer of 100 trajectories with a decreasing learning rate starting at 0.02. 25 trajectories are left out for validation on each epoch. The training is terminated when the validation loss is not decreasing more than 3 epochs in a row. After that, 30% of the buffer is replaced with new trajectories, and training continues.

We also incorporated some notion of random variables in hidden states by splitting the hidden state of the tested LSTM into groups. In all experiments the hidden state represents 10 categorical variables with 10 states. That is, LSTM is forced to learn 10 categorical distributions with multi-cross-entropy loss to explain the observed sequences, which is a somewhat close to the multi-categorical hidden state representation used in DreamerV2/V3 [35]. The idea of using symexp activation function, mentioned above, is inspired by Dreamer too, and is used to remedy the problem of learning extreme probability values. Without symexp the neural network has to represent zero probability with high

negative logit values and one-probability with high positive logit values, which is hard to reach with low learning rate and may lead to instabilities. Thus, symexp function makes it faster to reach target values in log space.

## D.2 CSCG

CSCG baseline was implemented using code from the repository accompanying the paper ([https://github.com/vicariousinc/naturecomm\\_cscg](https://github.com/vicariousinc/naturecomm_cscg)). CSCG with 10 clones per observation state was trained on batches with a size of 2500 observation steps for Gridworld tasks with 1000 EM algorithm iterations. We iteratively calculated the exponential moving average of transition matrices obtained for different batches with a smoothing coefficient  $\alpha = 0.9$  as described in the paper [51]. This smoothed transition matrix was used as an initialization for the next training batch and for inference. The first batch of observations is gathered using the uniform policy, and later batches are gathered using the current best policy. In so-called oracle mode, after the environment changes, the agent gathers a uniform policy batch again.

## D.3 DHTM

In the POMDP Gridworld task, a graph for DHTM consists of three hidden variables  $H$  with 40 cells per feature state, which is raw observation with 7 states in the case of Gridworld. Each hidden variable gets the same observation, and their predictions are averaged. Using several hidden variables here is essential, as it significantly increases the amount of trajectories memory is able to store by decreasing collision probability for hidden state representations of different trajectories. The same graph is used for the AnimalAI task, but with the encoder block forming one feature variable with 50 states.

In MDP Gridworld, a graph with one hidden variable and one cell for observation state is used, as there is no need to distinguish observations in different contexts.

Generally, the softmax strategy much better fits DHTM than Epsilon greedy. This is connected with the hidden state generalization problem discussed in Section 5. Each new trajectory creates a new hidden state, for which possible future trajectories are not known. The more exploration there is, the less useful the memory is. Softmax renders exploration more narrowed around already-known good trajectories, allowing better reuse of DHTM’s knowledge.

SFs are formed using  $\gamma = 0.8$  in all experiments except MDP Gridworld, where  $\gamma = 0.99$  is used. The maximum planning horizon is set to 50 in POMDP Gridworld and AnimalAI, with stopping criteria based on predicted feature variable distribution: 1) DKL between prediction and uniform distribution is less than 0.1, 2) net probability of feature states with positive rewards is greater than 0.01. For MDP Gridworld, planning steps are fixed and equal to 10. The same SF parameters were used for CSCG and LSTM.

In all experiments, segments are initialized with the maximum value, which is 1. Synapses are initialized with 0.5. Segments’ and synapses’ learning rates are 0.1. We also prune segments with values less than 0.3 to speed up learning.

# E Experimental Setups

## E.1 Gridworld

We use a simple homebrew Gridworld implementation. Each Gridworld position maps to a colour, reward, and terminal state indicator. There are two special colours for the world border and obstacles. Each timestep, an agent gets the colour index of the current agent’s position. In MDP mode, the agent gets a tuple of its coordinates in the maze. An agent is able to see obstacles or border colour when trying to go through them. We also punish an agent trying to go through a wall or world border in addition to base step reward punishment to facilitate faster convergence to optimal trajectories.

Setups used in our experiments are depicted in Figures 7 and 8. Here, the red colour corresponds to obstacles and the light gray colour to the reward. In each episode, the agent and the terminal rewarding state have the same initial positions. The episode ends when the terminal state is entered or the limit of action steps is reached.

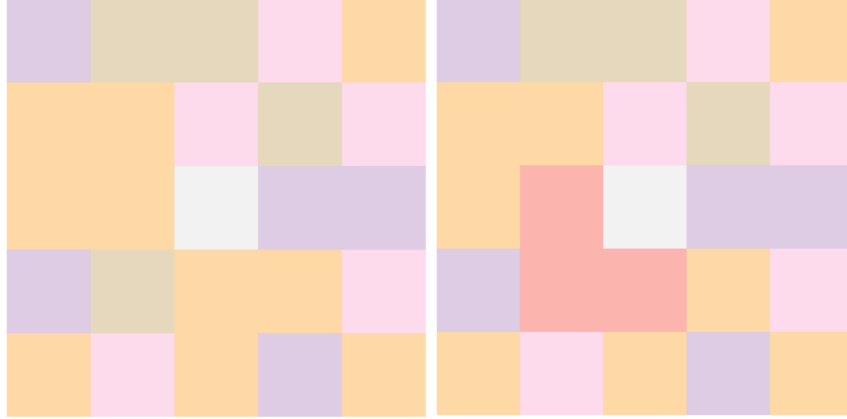


Figure 7: Schematic view of MDP Gridworld setups, in which agent gets its Gridworld position instead of colour index. The left picture shows the initial setup of the environment, with the reward in the center. The right picture represents the environment after the reward is blocked by obstacles (red squares). Agent’s initial position in the lower left corner.

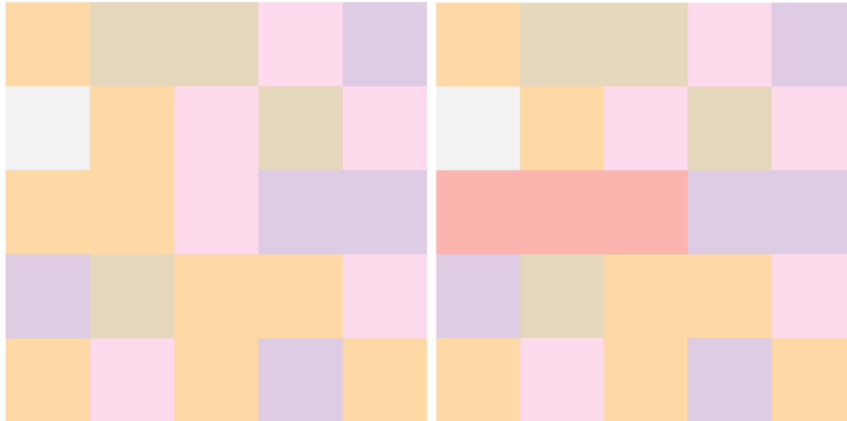


Figure 8: Schematic view of POMDP Gridworld setups. The left picture shows the initial setup of the environment, with the reward delivered by the light gray square. The right picture represents the environment after the reward is blocked by obstacles (red squares). Agent’s initial position in the lower left corner.

## E.2 AnimalAI

AnimalAI is a testbed inspired by experiments with animals [36]. The environment consists of 3D area surrounded by a wall and many different objects that can be placed using a configuration file, including walls, food, ramps, trees, movable obstacles, and more. We tested our agent in a 10x10-meter room surrounded by walls (see Fig. 9). Each timestep, the agent gets an RGB image of a first-person view of the environment and is able to influence its behaviour by choosing one of three actions: turn left, turn right, or go forward. The agent and food item have the same fixed initial positions for each episode. The episode ends if the food item is collected or the maximum episode time is reached. To make an agent’s actions more discretized, we repeat its choice three times and skip three frames.

## F Glossary

**Categorical Random Variable**—a discrete random variable that can take on of finite  $K$  possible states.

**Cortical Column or Minicolumn**—a population of neurons in the neocortex that spans across layers



Figure 9: Sample of the agent’s first-person view of our setup in AnimalAI environment. The green ball represents a goal, a food item to be collected.

and shares sensory input.

**Dendritic segment**—a group of synapses (neuron’s connections) that acts as an independent computational unit affecting the resulting neuron’s activity.

**Factor Graph**—bipartite graph representing the factorization of a probability distribution, with one part representing factor nodes and another—random variables.

**Hidden Markov Model (HMM)**—statistical model of a stochastic process where state probability depends only on previous state of the process.

**Multi-compartment neuron model**—a model of neuron that divides neuron’s connections into groups (segments) of different types (compartments), where each group may be considered as partly independent computational unit and groups of each compartment may affect the neuron’s activity differently.

**Sparse Distributed Representations (SDR)**—sparse binary vector in a high-dimensional space, usually formed by k-WTA algorithms.

**Spatial Pooler (SP)**—a distributed noise-tolerant online clustering neural network algorithm that converts input binary patterns into SDRs with fixed sparsity while retaining pairwise similarity.

**Successor Representations (SR)**—a discounted sum of future [one-hot encoded] observations.

**Successor Features (SF)**—a generalization of SR, a discounted sum of future latent states.

**Temporal Memory (TM)**—in this work by this term we mean “memory for sequences”.